
CHAMP: Conformalized 3D Human Multi-Hypothesis Pose Estimators

Harry Zhang, Luca Carlone
Massachusetts Institute of Technology
Cambridge, MA 02139, USA
{harryz, lcarlone}@mit.edu

Abstract

We introduce CHAMP, a novel method for learning sequence-to-sequence, multi-hypothesis 3D human poses from 2D keypoints by leveraging a conditional distribution with a diffusion model. To predict a single output 3D pose sequence, we generate and aggregate multiple 3D pose hypotheses. For better aggregation results, we develop a method to score these hypotheses during training, effectively integrating conformal prediction into the learning process. This process results in a differentiable conformal predictor that is trained end-to-end with the 3D pose estimator. Post-training, the learned scoring model is used as the conformity score, and the 3D pose estimator is combined with a conformal predictor to select the most accurate hypotheses for downstream aggregation. Our results indicate that using a simple mean aggregation on the conformal prediction-filtered hypotheses set yields competitive results. When integrated with more sophisticated aggregation techniques, our method achieves state-of-the-art performance across various metrics and datasets while inheriting the probabilistic guarantees of conformal prediction.

1 Introduction

Learning to estimate 3D human poses from videos is an important task in computer vision and robotics. Typical 3D human pose estimators learn to predict a single 3D human pose from an RGB image, either in an end-to-end manner or by relying on pre-existing 2D keypoint detection methods applied to the RGB images. Recent advances in sequence-to-sequence modeling enable learning 3D human poses in sequence by using RGB videos, which significantly improves the flexibility and efficiency of such estimators (Zhang et al., 2022b,a). While promising, such approaches only focus on *single-hypothesis* predictions, which is an inherently ill-posed problem when trying to reconstruct a 3D human pose given inputs collected from one viewpoint.

Thus, a more recent line of work focuses on learning *multi-hypothesis* 3D human pose estimators from 2D inputs. Instead of learning one deterministic target, such methods model the 2D-to-3D pose learning problem as learning a conditional distribution, which describes the distribution of the 3D poses given 2D inputs. This change in problem formulation prompts the use of generative models such as GANs, VAEs, and Diffusion models (Li & Lee, 2020; Sharma et al., 2019; Shan et al., 2023), which can propose multiple hypotheses of 3D poses given a single 2D input. For practical uses, one should also consider aggregating the hypotheses to generate one single output prediction. However, due to the imperfection of the trained generative models, using all hypotheses when aggregating could be inefficient and suboptimal if some are exceedingly inaccurate.

To counter the aforementioned problems, we take inspiration from an important tool in statistical learning, conformal prediction (CP) (Shafer & Vovk, 2008; Angelopoulos & Bates, 2021), which uses a *post-training* calibration step to guarantee a user-specified coverage: by allowing to predict

confidence sets $C(X)$, CP guarantees the true value Y to be included with confidence level α , i.e. $P(Y \in C(X)) \geq 1 - \alpha$ when the calibration examples $(X_i, Y_i) \in I_{\text{cal}}$ are drawn exchangeably from the test distribution. There are typically two steps involved in the CP process: In the calibration step, the conformity scores on the calibration set are ranked to determine a cut-off threshold τ for the predicted values guaranteeing coverage $1 - \alpha$, usually via quantile computation. In the prediction step, conformity scores, which measure the conformity between the output and possible ground-truth values, are computed to construct the confidence sets $C(X)$ by using the calibrated threshold τ . CP

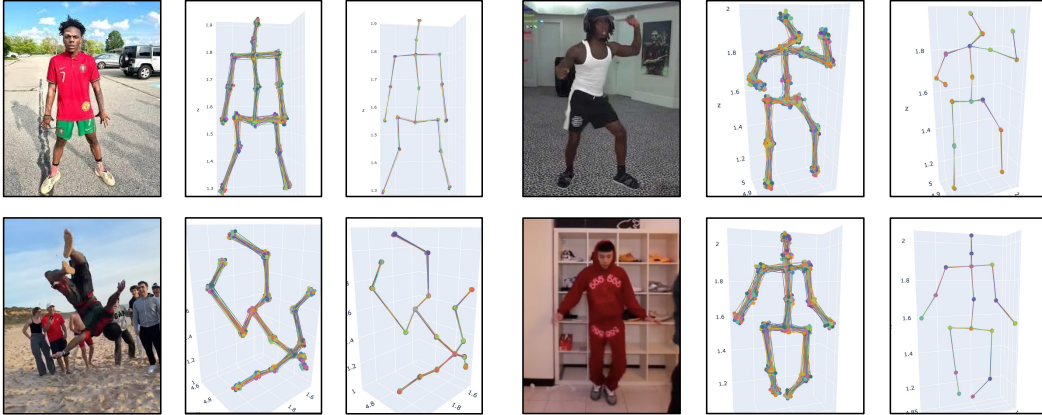


Figure 1: CHAMP sample results obtained on in-the-wild videos collected from TikTok. Having observed 2D keypoints, CHAMP proposes multiple hypotheses of the 3D human skeleton poses, and then a conformal predictor trained end-to-end with the pose estimator refines the confidence set by filtering out low-conformity-score hypotheses. This smaller set will be used in downstream aggregation for a single output prediction.

is highly flexible as it can be applied to any machine learning model. However, since it is applied post-training, learning the model parameters is not informed about the *post-hoc* conformalization step: the model is not tuned towards any specific CP objective such as reducing expected confidence set size (inefficiency). To bias the training towards lower inefficiency, ConfTr (Stutz et al., 2021) proposes a fully differentiable CP operation for classification tasks, which is applied end-to-end with the prediction model and optimizes a differentiable inefficiency loss in tandem with the original class loss for the classifier. This operation allows the model to learn parameters to reduce the inefficiency of the confidence set size during conformalization. Inspired by this, we wish to learn a scoring model that scores the “quality” of each hypothesis by measuring its conformity to the ground truth. We can then use this scoring model to simulate CP and optimize for the inefficiency in a differentiable manner, as done in (Stutz et al., 2021). During test time, we propose a large number of hypotheses and do regular CP to filter out the low-score ones before feeding into the downstream aggregation steps. The learned CP procedure can be applied to any multi-hypothesis estimator training process to refine the hypotheses confidence set size during test time for better aggregation results. With this learned CP wrapper, we present **CHAMP**, a Conformalized 3D **Hu**mAn **Mu**lti-**Hypo**theses **Po**se **E**stimator. To summarize, the contributions of this work include:

- A novel sequence-to-sequence, multi-hypothesis 3D human pose estimator from 2D keypoints.
- A novel method to conformalize 3D human pose estimates during training by learning a score function to rank the quality of the proposed hypotheses.
- A novel method to aggregate the multiple hypotheses from the estimator output using conformalization based on a learned score function.
- Quantitative and qualitative results that demonstrate the state-of-the-art results of our method on a variety of real-world datasets.

2 Related Work

Diffusion Models are a family of generative models that gradually corrupt data by adding noise, and then learn to recover the original data by reversing this process (Sohl-Dickstein et al., 2015; Ho et al., 2020; Song & Ermon, 2020; Song et al., 2020). They have achieved success in generating high-fidelity samples in various applications such as image generation (Ho et al., 2022; Saharia

et al., 2022; Nichol et al., 2021; Batzolis et al., 2021; Rombach et al., 2022; Zhang et al., 2020), multi-modal learning (Levkovitch et al., 2022; Kim et al., 2022; Huang et al., 2022; Avrahami et al., 2022; Zhang et al., 2021) and pose estimations in 3D vision problems (Gong et al., 2023; Wu et al., 2023; Devgon et al., 2020). We use Diffusion models to learn 3D human poses from 2D keypoints.

3D Human Pose Estimation is an important problem in computer vision and robotics. With deep learning, various end-to-end approaches have been proposed (Tekin et al., 2016; Pavlakos et al., 2017; Elmquist et al., 2022). However, with the maturity of 2D human keypoints detection, (Ho et al., 2022; Cao et al., 2017; Ma et al., 2022; Zhang, 2016; Sim et al., 2019), more robust approaches focus on uplifting 2D keypoints to 3D, resulting in better performance (Martinez et al., 2017; Zhou et al., 2017; Xu & Takano, 2021; Zhao et al., 2019; Lim et al., 2021, 2022), where one typically deals with a frame-to-frame problem, or a sequence-to-sequence problem. Being able to predict a 3D keypoints sequence directly from a 2D keypoint sequence is highly desirable as it has higher efficiency and flexibility. In this scheme, deterministic methods learn to predict one single 3D output from the 2D input (Pavlo et al., 2019; Zeng et al., 2020; Zheng et al., 2021; Shan et al., 2021; Jin et al., 2024; Hu et al., 2021; Zhan et al., 2022; Eisner et al., 2022). However, with a single viewpoint, such a formulation is ill-posed because there could be many possible 3D poses satisfying the same 2D keypoint configuration. Thus, it is desirable to model the problem as a conditional probability distribution. Deep generative models have shown great potential in modeling such distributions. Specifically, mixed-density network (Li & Lee, 2019; Pan et al., 2022, 2023), VAE (Sharma et al., 2019; Zhang et al., 2023), normalizing flows (Wehrbein et al., 2021), GAN (Li & Lee, 2019), and Diffusion models (Feng et al., 2023; Choi et al., 2023; Rommel et al., 2023; Avigal et al., 2021; Yao et al., 2023; Shen et al., 2024) have all been applied to modeling such conditional distribution. In our work, we use (Zhang et al., 2022b) as the backbone for generating 3D keypoints sequences from 2D keypoints sequences. To infer multiple hypotheses, we follow the frameworks in (Shan et al., 2023; Gong et al., 2023; Zhou et al., 2023) to learn to recover 3D pose hypotheses from Gaussian noises.

Conformal Prediction (CP) is a powerful and flexible distribution-free uncertainty quantification technique that can be applied to any machine learning model (Angelopoulos & Bates, 2021; Shafer & Vovk, 2008). Assuming the exchangeability of the calibration data, CP has desirable coverage guarantees. Thus, it has been applied to many fields such as robotics (Huang et al., 2023; Avigal et al., 2020; Sun et al., 2024), pose estimation (Yang & Pavone, 2023), and image regression (Teneggi et al., 2023; Angelopoulos et al., 2022). More sophisticated CP paradigms have been also proposed to tackle distribution shift and online learning problems (Angelopoulos et al., 2024; Gibbs & Candès, 2022; Bhatnagar et al., 2023; Feldman et al., 2022). Since CP is applied post-training, the learned model is not aware of such conformalization during training. To gain better control over the confidence set of CP, learning conformal predictors and nonconformity score end-to-end with the model has been proposed in (Stutz et al., 2021; Fisch et al., 2021; Bai et al., 2022). More closely related to our proposal is the work of (Stutz et al., 2021), but instead of using raw logits as the conformity score for classification, we learn an extra scoring model as the score to rank the hypotheses and simulate CP during training.

3 Problem Formulation

We are interested in the problem of learning a sequence of 3D human poses from a sequence of 2D human pose keypoints. We assume the 2D keypoints are available to us, which could be detected from the RGB images using well-established methods such as (Li et al., 2022b). Formally, given the input 2D keypoints sequence $\mathbf{x} = \{\mathbf{p}_n^{2d} | n = 1, \dots, N\}$, where $\mathbf{p}_n^{2d} \in \mathbb{R}^{J \times 2}$, our goal is to learn a conditional distribution for the possible corresponding 3D positions of all joints $p_\theta(\mathbf{y}|\mathbf{x})$, where the sequence $\mathbf{y} = \{\mathbf{p}_n^{3d} | n = 1, \dots, N\}$ and $\mathbf{p}_n^{3d} \in \mathbb{R}^{J \times 3}$. Here, N represents the number of input and output frames and J is the number of human joints in each frame. With the learned distribution $p_\theta(\mathbf{y}|\mathbf{x})$, we are able to do inference and generate hypotheses of 3D poses $\mathbf{H}_\mathbf{y} \in \mathbb{R}^{H \times N \times J \times 3}$, where H is the number of the hypotheses. We then conformalize the hypotheses to select the higher-quality ones and aggregate the latter in order to obtain a single estimate $\tilde{\mathbf{y}}$ as the final output.

4 Methods

We use a Diffusion model (Ho et al., 2020) to learn the conditional distribution $p_\theta(\mathbf{y}|\mathbf{x})$ due to its capability of modeling complex distributions and producing high-quality samples. With the trained diffusion model, we are able to generate many hypotheses sequences and aggregate them to produce

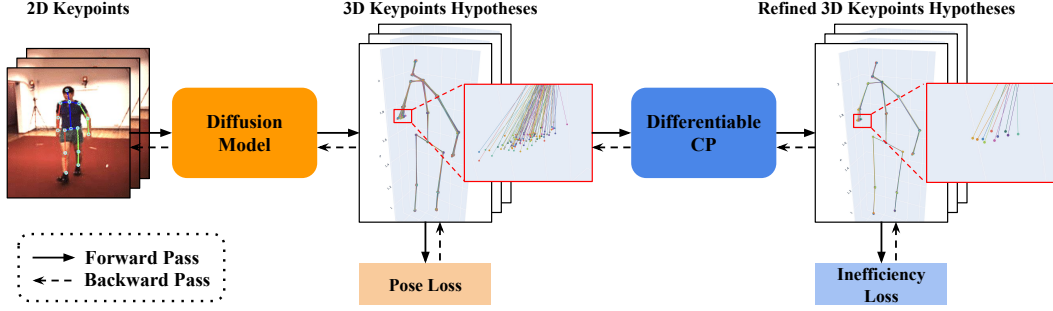


Figure 2: CHAMP Overview. CHAMP takes as input a sequence of 2D keypoints detected on a series of input RGB video frames. The 2D keypoints sequence gets fed into a Diffusion model to produce 3D keypoints hypotheses for the sequence. The output of the Diffusion model is supervised via a Pose Loss. Then we apply differentiable CP end-to-end during training on the hypotheses sequences, resulting in a smaller confidence set. The confidence set is used to calculate an Inefficiency Loss during training. Note that we show one frame in the sequence and hard assignment for the confidence set during training for better interpretability.

a robust single prediction sequence for the final output. Moreover, we would like to make the model itself aware of the *post-hoc* hypotheses aggregation step so that the aggregation step does not get skewed by low-quality hypotheses. Thus, there should be an extra component in the model to shape the hypotheses confidence set. To achieve this, we learn an extra scoring model to rank the hypotheses and optimize the size of the hypotheses confidence set thresholded by the 90% quantile score, effectively simulating conformal prediction during training, illustrated in Fig. 2.

4.1 Learning 3D Human Poses with a Diffusion Model

The use of Diffusion models in 3D human pose estimation has been shown effective in various previous works (Feng et al., 2023; Gong et al., 2023; Shan et al., 2023; Choi et al., 2023), and we adapt the same paradigm in modeling the forward and the reverse process for the Diffusion model.

Forward Process. In the forward process, the Diffusion model takes as input a ground-truth 3D human pose sequence $\mathbf{y}_0 \in \mathbb{R}^{N \times J \times 3}$ and a sampled time step $t \sim \text{Unif}(0, T)$, where T is the maximum number of diffusion steps. Then the forward process gradually diffuses the input by adding independent Gaussian noises $\epsilon \sim \mathcal{N}(0, \mathbf{I})$ at each step. The nice property reported in (Ho et al., 2020) shows that the process can be succinctly written as:

$$q(\mathbf{y}_t | \mathbf{y}_0) = \sqrt{\bar{\alpha}_t} \mathbf{y}_0 + \sqrt{1 - \bar{\alpha}_t} \epsilon \quad (1)$$

where $\bar{\alpha}_t$ is a constant depending on the cosine variance schedule.

Reverse Process. To train such a Diffusion model, in the reverse process, we denoise the corrupted 3D pose sequence \mathbf{y}_t . While the derivation in (Ho et al., 2020) simplifies the ELBO objective to minimizing the distance between the injected noise ϵ_t and a learned noise $\epsilon_\theta(\sqrt{\bar{\alpha}_t} \mathbf{y}_0 + \sqrt{1 - \bar{\alpha}_t} \epsilon_t, t)$, we frame the problem slightly differently, following (Shan et al., 2023). Instead of training a network to learn the injected noise, we train a denoiser model D_θ that outputs the predicted pose $\bar{\mathbf{y}}_0$ directly:

$$\bar{\mathbf{y}}_0 = D_\theta(\mathbf{y}_t, x, t) \quad (2)$$

where the denoiser model takes as input the corrupted 3D pose sequence, the input 2D keypoints sequence, and the diffusion step to recover the uncorrupted input pose sequence $\bar{\mathbf{y}}_0$. We then supervise the predicted sequence with the ground-truth sequence using the mean per-joint MSE:

$$\mathcal{L}_{\text{pose}} = \frac{\|\mathbf{y}_0 - \bar{\mathbf{y}}_0\|_2^2}{N \cdot J} \quad (3)$$

Denoiser Model. We build upon the MixSTE model (Zhang et al., 2022b) as the denoiser model in the reverse process of the Diffusion model. MixSTE uses two separate attention mechanisms, effectively learning spatial and temporal relationships of the keypoints sequence in a modular way by combining several spatial and temporal attention blocks. To condition the MixSTE network on the corrupted 3D keypoints sequence, we change the network input by concatenating 2D keypoints

and noisy 3D poses and we add a diffusion timestep embedding after the input embedding in the first attention block. A detailed description of the denoiser model is given in Appendix B and D.

Generating Hypotheses. Using the denoiser model, which models the conditional distribution $p_\theta(\mathbf{y}|\mathbf{x})$, we are able to generate a number of hypotheses during inference. Following the reverse process of the Diffusion model, we obtain the hypotheses set $\mathbf{H}_y = \{\bar{\mathbf{y}}^1, \bar{\mathbf{y}}^2, \dots, \bar{\mathbf{y}}^H\}$ of size H by sampling standard normal noises $\mathbf{y}_T^h \sim \mathcal{N}(0, \mathbf{I}) \in \mathbf{R}^{N \times J \times 3}$, where the superscript $h = [1, 2, \dots, H]$ indexes the hypotheses, and feeding them into the denoiser model D_θ :

$$\bar{\mathbf{y}}^h = D_\theta(\mathbf{y}_T^h, \mathbf{x}, T) \quad (4)$$

4.2 Learning Conformalization for the Hypotheses Confidence Set

While we are able to generate arbitrarily large numbers of hypotheses during test time with the distribution learned by the Diffusion model, we still need to aggregate the proposed hypotheses into a single prediction. The correct way to aggregate the hypotheses remains an open problem. Taking a naive average would be suboptimal as the existence of outliers in the proposed hypotheses might skew the average. Other approaches improve the aggregation step by selecting the hypotheses that result in closer distances to 2D keypoints after projection via camera matrices, but still retain a large set of hypotheses before the aggregation step (Shan et al., 2023).

Conformal Prediction. A possible solution is to *conformalize* the hypotheses using conformal prediction (CP). Conformal prediction produces a set of predictions which covers the ground truth with high probability: given a trained prediction model f_θ , conformal prediction first calibrates a cutoff value τ by ranking a calibration set I_{cal} given each component’s *conformity score* $\phi(\mathbf{y}_{\text{cal}}, \mathbf{y}_{\text{GT}})$ and setting the cutoff value as the user-specified $(1 + 1/|I_{\text{cal}}|)\alpha$ -quantile of the calibration set scores. After the calibration step, the generic threshold conformal predictor constructs the conformal prediction set as follows:

$$C(\mathbf{x}, \tau) = \{\mathbf{y} : \phi(\mathbf{y}, f_\theta(\mathbf{x})) \geq \tau\} \quad (5)$$

With a properly selected conformity score function ϕ , as well as a user-specified coverage parameter α , the **post-training** conformal prediction guarantees the true value to be included in $C(\mathbf{x}, \tau)$ with confidence level α , i.e. $P(\mathbf{y}_{\text{GT}} \in C(\mathbf{x}, \tau)) \geq \alpha$. A key metric for a conformal predictor is the size of the confidence set $C_\theta(\mathbf{x}, \tau)$, or *inefficiency*: a good confidence set should be large enough to cover the ground truth, and small enough to be informative (low inefficiency). A very large confidence set could cover the ground truth with high probability, but it might not be necessarily useful as it is inefficient to consider a lot of possible values (high inefficiency). Given H hypotheses of 3D human pose sequences, we wish to use the threshold conformal predictor above to refine the hypotheses set, resulting in H' “good” hypotheses, where $H' \leq H$. Essentially, we wish to have a *low-inefficiency* conformal predictor, which selects a smaller number of elite hypotheses from the set for downstream aggregation. CP is intended to be used as a “wrapper” around the prediction model, and we wish to achieve better, fine-grained control over the inefficiency of the CP wrapper for downstream aggregation, conditioned on the input 2D and output 3D human pose sequence data. Thus, inspired by (Stutz et al., 2021), we integrate CP into the training, optimizing for the inefficiency of the confidence set online by simulating CP **during training** in a differentiable manner.

Learning CP via Inefficiency Optimization. We build on top of the ConfTr paradigm proposed in (Stutz et al., 2021). We first design a conformity score function for poses. Unlike (Yang & Pavone, 2023), where the score function ϕ is hand-designed, we wish to learn a conformity score function ϕ_θ that measures the distance between the proposed hypothesis and the ground truth. During training, we propose H_{train} predicted output sequences as the hypotheses for each input 2D keypoints sequence in the mini-batch. To implement the score function, we reuse the input embedding layer of the modified MixSTE and further project the embeddings into two lower-dimensional tensors with an extra MLP for the hypothesis and the ground-truth 3D pose sequence respectively and then calculate the cosine similarity between the two embeddings. Thus, a higher score function output means the hypothesis is more similar to the ground-truth 3D pose sequence in the embedding space. Formally, the conformity score between the hypothesis 3D pose sequence $\bar{\mathbf{y}}^h$ and the ground-truth 3D pose sequence \mathbf{y}_{GT} is measured as:

$$\phi_\theta(\bar{\mathbf{y}}^h, \mathbf{y}_{\text{GT}}) = \frac{s_\theta(\mathbf{IE}_\theta(\bar{\mathbf{y}}^h))^\top s_\theta(\mathbf{IE}_\theta(\mathbf{y}_{\text{GT}}))}{\|s_\theta(\mathbf{IE}_\theta(\bar{\mathbf{y}}^h))\| \cdot \|s_\theta(\mathbf{IE}_\theta(\mathbf{y}_{\text{GT}}))\|} \quad (6)$$

where s_θ is the extra MLP in the conformity score model and IE_θ is the input embedding layer of the denoiser model. With the conformity score model output, we perform differentiable CP on each mini-batch of size B during training. Similar to (Stutz et al., 2021), we split each set of H_{train} hypotheses of the mini-batch in half: the first half, \mathbf{H}_{cal} , is used for calibration, and the second half, \mathbf{H}_{pred} , for prediction and loss computation. On \mathbf{H}_{cal} , we calibrate τ by computing the $(1 + 1/|\mathbf{H}_{\text{cal}}|)^\alpha$ -quantile of the conformity scores in a differentiable manner. This is done using a smooth sorting operation, which has been widely studied in (Blondel et al., 2020) and (Cuturi et al., 2019). On \mathbf{H}_{pred} , we calculate the soft inefficiency score by using the *soft* assignment of hypothesis $\bar{\mathbf{y}}^h$ being in the prediction set given the quantile threshold τ :

$$C_\theta(\bar{\mathbf{y}}^h, \tau) := \sigma\left(\frac{\phi_\theta(\bar{\mathbf{y}}^h, \mathbf{y}_{\text{GT}}) - \tau}{\mathcal{T}}\right) \quad (7)$$

where σ here is the sigmoid function and \mathcal{T} is the temperature hyperparameter. When $\mathcal{T} \rightarrow 0$, we recover the *hard* assignment and $C_\theta(\bar{\mathbf{y}}^h, \tau) = 1$ if $\phi_\theta(\bar{\mathbf{y}}^h, \mathbf{y}_{\text{GT}}) \geq \tau$ and 0 otherwise. Thus, we are able to measure the size of the CP set of the hypotheses by $\sum_h C_\theta(\bar{\mathbf{y}}^h, \tau)$. On \mathbf{H}_{pred} , we compute $C_\theta(\bar{\mathbf{y}}^h, \tau)$ and then calculate the differentiable inefficiency score:

$$\Omega(C_\theta(\mathbf{H}_{\text{pred}}, \tau)) = \max\left(\sum_{h=1}^{|\mathbf{H}_{\text{pred}}|} C_\theta(\bar{\mathbf{y}}^h, \tau) - \kappa, 0\right) \quad (8)$$

where κ is a hyperparameter that avoids penalizing singletons. With the differentiable inefficiency score defined, we are able to optimize for the expected inefficiency across batches during training:

$$\mathcal{L}_{\text{ineff}} = \log \mathbb{E}[\Omega(C_\theta(\mathbf{H}_{\text{pred}}, \tau))] \quad (9)$$

Full Training Objective. The computational graph of this loss involves the denoiser model input embedding, and since every operation is made differentiable by construction, we are able to back-propagate the inefficiency loss into the model, further shaping the model on top of the original pose loss. The final training objective of our model is thus:

$$\mathcal{L} = \mathcal{L}_{\text{pose}} + \lambda \mathcal{L}_{\text{ineff}} \quad (10)$$

where λ is a hyperparameter representing the weight of the inefficiency loss.

4.3 Conformalized Inference

During inference, to retain the coverage guarantee of CP, any CP method can be applied to re-calibrate τ on a held-out calibration set I_{cal} as usual, i.e., the thresholds τ obtained during training is not kept during test time. Given a trained pose estimation denoiser model D_θ and the conformity scoring model ϕ_θ trained end-to-end with D_θ , for each testing 2D keypoints sequence, \mathbf{x} , we wish to construct a hypotheses confidence set for the downstream aggregation as follows:

$$C_\theta(\mathbf{y}, \tau) = \{\mathbf{y} : \phi_\theta(\tilde{\mathbf{y}}, \mathbf{y}) \geq \tau\} \quad (11)$$

where $\tilde{\mathbf{y}}$ is obtained via eq. (4) and $\mathbf{y}_T \sim \mathcal{N}(0, \mathbf{I})$. In practice, we take the mean of 20 $\tilde{\mathbf{y}}$. To generate candidate hypotheses for the hypotheses confidence set, we sample from the learned distribution $p_\theta(\mathbf{y}|\mathbf{x})$ H times using (4) and refine them using (11), resulting in a smaller hypotheses set \mathbf{H}_y of size H' . We then aggregate the set \mathbf{H}_y to obtain a single output for practical use.

5 Experiments

To evaluate our method, we train and test on standard human pose estimation datasets and provide quantitative results. We also provide qualitative results on in-the-wild videos.

Human3.6M (Ionescu et al., 2013) is the standard and the largest indoor dataset for 3D human pose estimation. The dataset collects videos from 11 actors engaging in 15 activities and the pose sequence videos are captured by 4 synchronized and calibrated cameras at 50Hz. Similar to (Shan et al., 2023; Zhang et al., 2022b), we train on 5 actors (S1, S5, S6, S7, S8) and evaluate on 2 actors (S9, S11). Quantitatively, following the standard evaluation scheme, we report the mean per

joint position error (MPJPE), which is often referred to as Protocol #1, which computes the mean Euclidean distance between estimated and ground truth 3D joint positions in millimeters. We also provide Protocol #2 results in Appendix E.

MPI-INF-3DHP (Mehta et al., 2017) is a more challenging dataset consisting of indoor and outdoor activities, from 14 camera views which cover a greater diversity of poses. The training set contains 8 activities, and the test set contains 6. We preprocess the dataset with the valid frames provided by the authors for testing, following (Zhang et al., 2022b; Shan et al., 2023; Gong et al., 2023). Quantitatively, we report MPJPE, the percentage of correct keypoints (PCK), which describes the percentage of keypoints with Euclidean error less than 150mm, as well as the AUC score for this percentage.

For both of the datasets, in our setting, we hold out 2% of the training dataset for conformal calibration during test time. The held-out calibration set is not seen by the network during training. We compare 4 variations of our method. The backbone (weights) of the variations and the training process remain the same, but the key difference lies in the aggregation step during test time:

- **CHAMP-Naive:** Trained with inefficiency loss, but for multi-hypothesis scenarios, during test time, we do not refine the hypotheses set with CP, and we use all hypotheses with a mean aggregation. In single-hypothesis scenarios, we only propose 1 hypothesis as the output.
- **CHAMP:** Same backbone as CHAMP-Naive, but only aggregates refined hypotheses confidence set in eq. (11) via mean aggregation.
- **CHAMP-Agg:** Instead of taking the average, we use the J-Agg method from (Shan et al., 2023) on the set in eq. (11), which uses known or estimated intrinsic camera parameters to reproject 3D hypotheses to the 2D camera plane and selecting the joint hypotheses with the minimum projection error.
- **CHAMP-Best:** We use J-Best method in (Shan et al., 2023) on the set in eq. (11), which selects the joint hypothesis that is closest to the ground truth, and then combines the selected joints into the final 3D pose. This is the upper bound of J-Agg performance.

5.1 Results on Human-3.6M

We discuss the quantitative results on the Human-3.6M dataset. In the single-hypothesis setting, we set $H = 1$ to compare with other deterministic methods. While our method primarily focuses on multi-hypothesis scenarios, we propose 1 hypothesis and use the CHAMP-Naive variation, without using the conformal prediction pipeline. As the results suggest in Table 1, our method achieves performance on par with the current state-of-the-art methods in the single-hypothesis case.

In the multi-hypothesis setting, we set $H = 80$. CHAMP variants achieve SOTA results, especially when combined with more sophisticated aggregations proposed in D3DP (Shan et al., 2023). On average, without the conformal prediction pipeline, CHAMP-Naive is able to achieve 40mm MPJPE error and improves by 1.5mm when using conformal prediction and mean aggregation. Using J-Agg and J-Best, CHAMP gets further improved by 1.7mm and 3.6mm respectively.

Mean Per-Joint Position Error (Protocol #1) - mm																
	AVG.	Dir	Disc.	Eat	Greet	Phone	Photo	Pose	Pur.	Sit	SitD.	Smoke	Wait	WalkD.	Walk	WalkT.
Single Hypothesis																
Ray3D (Zhan et al., 2022)	49.7	44.7	48.7	48.7	48.4	51.0	59.9	46.8	46.9	58.7	61.7	50.2	46.4	51.5	38.6	41.8
STE (Li et al., 2022a)	43.6	39.9	43.4	40.0	40.9	46.4	50.6	42.1	39.8	55.8	61.6	44.9	43.3	44.9	29.9	30.3
P-STMO (Shan et al., 2022)	42.8	38.9	42.7	40.4	41.1	45.6	49.7	40.9	39.9	55.5	59.4	44.9	42.2	42.7	29.4	29.4
MixSTE (Zhang et al., 2022b)	41.0	37.9	40.1	37.5	39.4	43.3	50.0	39.8	39.9	52.5	56.6	42.4	40.1	40.5	27.6	27.7
DUE (Zhang et al., 2022a)	40.6	37.9	41.9	36.8	39.5	40.8	49.2	40.1	40.7	47.9	53.5	40.2	41.1	40.3	30.8	28.6
D3DP (Shan et al., 2023)	40.0	37.7	39.9	35.7	38.2	41.9	48.8	39.5	38.3	50.5	53.9	41.6	39.4	39.8	27.4	27.5
CHAMP-Naive (H=1)	40.2	39.5	40.3	35.8	38.7	42.2	48.7	40.2	38.2	50.3	53.2	41.5	39.2	40.2	26.9	27.3
Multiple Hypotheses																
MHFormer (Li et al., 2022b)	43.0	39.2	43.1	40.1	40.9	44.9	51.2	40.6	41.3	53.5	60.3	43.7	41.1	43.8	29.8	30.6
GraphMDN (Oikarinen et al., 2021)	61.3	51.9	56.1	55.3	58.0	63.5	75.1	53.3	56.5	69.4	92.7	60.1	58.0	65.5	49.8	53.6
DiffuPose (Choi et al., 2023)	49.4	43.4	50.7	45.5	50.2	49.6	53.4	48.6	45.0	56.9	70.7	47.8	48.2	51.3	43.1	43.4
DiffPose (Gong et al., 2023)	36.9	33.2	36.6	33.0	35.6	37.6	45.1	35.7	35.5	46.4	49.9	37.3	35.6	36.5	24.4	24.1
DiffPose (Feng et al., 2023)	43.3	38.1	43.3	35.3	43.1	46.6	48.2	39.0	37.6	51.9	59.3	41.7	47.6	45.5	37.4	36.0
D3DP-Agg (Shan et al., 2023)	39.5	37.3	39.5	35.6	37.8	41.4	48.2	39.1	37.6	49.9	52.8	41.2	39.2	39.4	27.2	27.1
CHAMP-Naive	40.0	39.4	40.1	35.4	38.2	42.0	48.5	40.0	38.1	50.1	52.9	43.4	39.1	39.9	27.7	28.2
CHAMP	38.5	36.5	38.9	34.2	37.1	40.1	46.9	38.2	36.5	47.9	50.7	40.1	37.6	37.6	25.7	26.4
CHAMP-Agg	36.0	36.2	36.1	30.9	31.8	39.5	43.6	35.1	33.9	43.1	47.2	39.9	34.9	36.1	25.1	25.9
D3DP-Best* (Shan et al., 2023)	35.4	33.0	34.8	31.7	33.1	37.5	43.7	34.8	33.6	45.7	47.8	37.0	35.0	35.0	24.3	24.1
CHAMP-Best*	34.9	35.9	35.2	30.3	31.4	37.4	42.9	34.4	33.5	41.5	46.9	37.9	34.8	34.8	24.5	24.6

Table 1: MPJPE (\downarrow) results on Human-3.6M dataset. Red: lowest error. Blue: second lowest error. In the single-hypothesis setting, our method runs without CP. In the multi-hypothesis setting, we compare four different variants of CHAMP as discussed in the main text. *Upper-bound performance, uses ground truth.

5.2 Results on MPI-INF-3DHP

We discuss the results on the MPI-INF-3DHP dataset in Table 2. In the single-hypothesis setting, CHAMP-Naive achieves results on par with other deterministic methods for the three metrics.

In the multi-hypothesis setting, we again set $H = 80$. CHAMP-Naive again yields fairly competitive results and when combined with conformal prediction and mean, J-Agg, and J-Best aggregation techniques, the performance continuously gets improved across the three metrics, with the CHAMP-Agg metric being the most competitive one, achieving SOTA results. These results here on this dataset follow the same trend as those on the Human3.6M dataset.

	PCK \uparrow	AUC \uparrow	MPJPE \downarrow
Single Hypothesis			
P-STMO (Shan et al., 2022)	97.9	75.8	32.2
MixSTE (Zhang et al., 2022b)	96.9	75.8	35.4
D3DP (Shan et al., 2023)	97.7	77.8	30.2
CHAMP-Naive	97.5	77.7	30.2
Multiple Hypotheses			
MHFormer (Li et al., 2022b)	93.8	63.3	58.0
DiffPose (Gong et al., 2023)	98.0	75.9	29.1
DiffPose (Feng et al., 2023)	94.6	62.8	64.6
D3DP-Agg (Shan et al., 2021)	97.7	78.2	29.7
CHAMP-Naive	97.5	78.1	29.9
CHAMP	97.9	78.4	29.1
CHAMP-Agg	98.0	78.6	28.6
D3DP-Best (Shan et al., 2021)	98.0	79.1	28.1
CHAMP-Best	98.2	79.1	28.0

Table 2: Results on the 3DHP dataset.

5.3 In-the-Wild Videos

To show the generalizability of our method to in-the-wild videos, we collect videos from YouTube, TikTok, and 3DPW dataset (Von Marcard et al., 2018). To construct 2D keypoints input, we use Cascaded Pyramid Network (Chen et al., 2018) fine-tuned on the Human3.6M dataset as the default weights are trained on MSCOCO (Lin et al., 2014), which has a slightly different skeleton structure. We directly apply the CHAMP model trained on the Human3.6M dataset to test on in-the-wild videos. Sample results are shown in Fig. 1, where the input videos are collected from TikTok. Qualitative results suggest that CHAMP is able to filter out outlier hypotheses using the conformity score function trained end-to-end with the pose estimation model. More results are shown in Appendix F.

5.4 Ablation Studies with Human3.6M Dataset

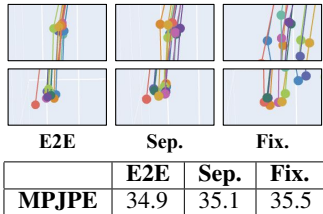


Figure 4: Comparison of conformity scores. **Top:** filtered hypotheses of two joints using the three scoring functions. **Bottom:** MPJPE (mm) values.

Choice of the Conformity Function. We compare our proposed end-to-end learned conformity score function with a separately trained conformity score function (Corso et al., 2022), and a hand-designed conformity score function. We compare the average performance across all actions on the Human3.6M dataset. For the separately trained conformity score function, we first only train the pose estimation backbone and generate 100 hypotheses per input sequence over a small subset of the training dataset. We then train the score function to predict if the proposed hypothesis conditioned on the input 2D keypoints results in an MPJPE of less than 25mm and use the ground-truth pose sequence as supervision. For the hand-designed conformity score, we use ϕ_{peak} from (Yang & Pavone, 2023), measuring the maximum MPJPE with respect to the ground truth across output frames. Note ϕ_{peak} measures “nonconformity”, so we negate such values to fit our setup. All three variants use the J-Best aggregation method. From Fig. 4, E2E score function yields the best performance and the two learned variants supersede the hand-designed version. In the two examples shown in Fig. 4, the filtered hypotheses seem to be more concentrated for learned score functions. It’s worth noting that all three variants result in competitive performance, demonstrating the importance of CP.

Number of Hypotheses. Another interesting ablation study to conduct is to ablate on the number of hypotheses during training (H_{train}) and inference (H). We compare the effects of H_{train} , H in Fig.

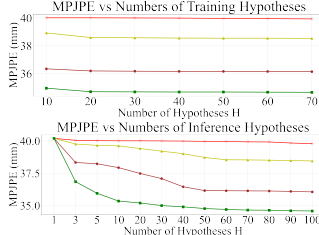


Figure 5: Comparison of #hypotheses in training and inference with 4 variants of CHAMP. **Red:** Naive, **Yellow:** CHAMP, **Brown:** Agg, **Green:** Best.

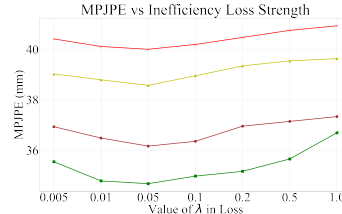


Figure 6: Comparison of λ in loss definition \mathcal{L} (Eq. 10) with 4 variants of CHAMP. **Red:** Naive, **Yellow:** CHAMP, **Brown:** Agg, **Green:** Best.

5, on the four variants of CHAMP. To compare the effect of H_{train} , we fix $H = 80$ and train a model for each value of hypotheses proposed during differentiable CP. Similarly, to compare the effect of H , we fix $H_{\text{train}} = 20$ during training and use the same model with different H during inference for CP. Results suggest that a good performance can be achieved with $H_{\text{train}} = 20$ during training, while any number higher than 20 brings marginal improvement and requires more GPU memory. Moreover, $H = 80$ during inference is sufficient for all four variants.

Strength of the Inefficiency Loss. Finally, we ablate on the value of λ in the overall training objective \mathcal{L} . This is an important ablation in that we can find suitable strength of the inefficiency loss $\mathcal{L}_{\text{ineff}}$ to make sure it does not conflict $\mathcal{L}_{\text{pose}}$. Results in Fig. 6 suggest that $\lambda = 0.05$ is the most efficient strength across all values, as smaller λ does not train the scoring model sufficiently and higher λ conflicts with the pose loss. This corroborates the smaller-scale hyperparameter sweep experiments we conducted before training the models.

5.5 Exchangeability and CP Guarantee

The inherent assumption of CP requires the calibration dataset to be exchangeable, which is weaker than asking them to be independent (Angelopoulos & Bates, 2021). This assumption typically fails when the calibration set is a single video sequence, where the image frames are temporally correlated. We learn a sequence-to-sequence model, where the input and output are long sequences of image frames from different videos, instead of single frames from the same video. This would drastically decrease the temporal correlation across the calibration dataset. Moreover, as shown in (Yang & Pavone, 2023), the video frames tend to be more independent if the videos are taken by multiple evenly spaced cameras, which is the case for our datasets of interest. We also investigate the empirical coverage of our method in Human 3.6M test set in Appendix A. Results suggest that we are able to inherit the coverage guarantee from CP with the learned conformity score even if the dataset is not fully exchangeable.

5.6 Implementation and Training Details

CHAMP’s denoiser model uses Adam optimizer with a weight decay parameter of 0.1 and momentum parameters $\beta_1 = \beta_2 = 0.99$. For the training objective in eq. (10), we use $\lambda = 0.05$. We train the CHAMP model using an NVIDIA V100 GPU, where the training process consumes an amortized GPU memory of 18GB, for 300 epochs with a batch size of 8 and a learning rate of $5e-5$ and reduce it on plateau with a factor of 0.5. Following previous work (Zhang et al., 2022b; Shan et al., 2021, 2023), we use input pose sequence of 243 frames ($N = 243$) of Human3.6M universal skeleton format. During training, the number of hypotheses is 20, and #DDIM iterations is set to 1. During inference, they are set to 80 and 10. The maximum number of diffusion steps is $T = 999$.

6 Limitations

While our method shows a promising improvement over the current 3D human pose estimation methods, it does have several limitations. First, the theoretical coverage guarantee of CP cannot be fully justified due to the input videos’ temporal correlation. Moreover, many hypotheses need to be proposed during training to improve the learned conformity score, which consumes a lot more GPU memory. Lastly, CHAMP only learns single-human 3D skeleton estimation, without considering dense, multi-human scenarios.

7 Conclusion

This work presents CHAMP, a novel method for learning multi-hypotheses 3D human poses with a learned conformal predictor from 2D keypoints. We empirically show that CHAMP achieves competitive results across multiple metrics and datasets, and when combined with more sophisticated downstream aggregation methods, it achieves state-of-the-art performance. Future work includes using more recent CP techniques that relax the exchangeability assumption (Barber et al., 2023), using more efficient sequence-to-sequence models such as Mamba (Gu & Dao, 2023), and scaling the pipeline up to dense, multi-human pose-shape joint prediction scenarios (Loper et al., 2023).

References

- Anastasios Angelopoulos, Emmanuel Candes, and Ryan J Tibshirani. Conformal pid control for time series prediction. *Advances in Neural Information Processing Systems*, 36, 2024.
- Anastasios N Angelopoulos and Stephen Bates. A gentle introduction to conformal prediction and distribution-free uncertainty quantification. *arXiv preprint arXiv:2107.07511*, 2021.
- Anastasios N Angelopoulos, Amit Pal Kohli, Stephen Bates, Michael Jordan, Jitendra Malik, Thayer Alshaabi, Srigoikul Upadhyayula, and Yaniv Romano. Image-to-image regression with distribution-free uncertainty quantification and applications in imaging. In *International Conference on Machine Learning*, pp. 717–730. PMLR, 2022.
- Yahav Avigal, Samuel Paradis, and Harry Zhang. 6-dof grasp planning using fast 3d reconstruction and grasp quality cnn. *arXiv preprint arXiv:2009.08618*, 2020.
- Yahav Avigal, Vishal Satish, Zachary Tam, Huang Huang, Harry Zhang, Michael Danielczuk, Jeffrey Ichnowski, and Ken Goldberg. Avplug: Approach vector planning for uncontact grasping amid clutter. In *2021 IEEE 17th International Conference on Automation Science and Engineering (CASE)*, pp. 1140–1147. IEEE, 2021.
- Omri Avrahami, Dani Lischinski, and Ohad Fried. Blended diffusion for text-driven editing of natural images. In *Proceedings of the IEEE/CVF Conference on Computer Vision and Pattern Recognition*, pp. 18208–18218, 2022.
- Yu Bai, Song Mei, Huan Wang, Yingbo Zhou, and Caiming Xiong. Efficient and differentiable conformal prediction with general function classes. *arXiv preprint arXiv:2202.11091*, 2022.
- Rina Foygel Barber, Emmanuel J Candes, Aaditya Ramdas, and Ryan J Tibshirani. Conformal prediction beyond exchangeability. *The Annals of Statistics*, 51(2):816–845, 2023.
- Georgios Batzolis, Jan Stanczuk, Carola-Bibiane Schönlieb, and Christian Etmann. Conditional image generation with score-based diffusion models. *arXiv preprint arXiv:2111.13606*, 2021.
- Aadyot Bhatnagar, Huan Wang, Caiming Xiong, and Yu Bai. Improved online conformal prediction via strongly adaptive online learning. In *International Conference on Machine Learning*, pp. 2337–2363. PMLR, 2023.
- Mathieu Blondel, Olivier Teboul, Quentin Berthet, and Josip Djolonga. Fast differentiable sorting and ranking. In *International Conference on Machine Learning*, pp. 950–959. PMLR, 2020.
- Zhe Cao, Tomas Simon, Shih-En Wei, and Yaser Sheikh. Realtime multi-person 2d pose estimation using part affinity fields. In *Proceedings of the IEEE conference on computer vision and pattern recognition*, pp. 7291–7299, 2017.
- Yilun Chen, Zhicheng Wang, Yuxiang Peng, Zhiqiang Zhang, Gang Yu, and Jian Sun. Cascaded pyramid network for multi-person pose estimation. In *Proceedings of the IEEE conference on computer vision and pattern recognition*, pp. 7103–7112, 2018.
- Jeongjun Choi, Dongseok Shim, and H Jin Kim. Diffupose: Monocular 3d human pose estimation via denoising diffusion probabilistic model. In *2023 IEEE/RSJ International Conference on Intelligent Robots and Systems (IROS)*, pp. 3773–3780. IEEE, 2023.
- Gabriele Corso, Hannes Stärk, Bowen Jing, Regina Barzilay, and Tommi Jaakkola. Diffdock: Diffusion steps, twists, and turns for molecular docking. *arXiv preprint arXiv:2210.01776*, 2022.
- Marco Cuturi, Olivier Teboul, and Jean-Philippe Vert. Differentiable ranking and sorting using optimal transport. *Advances in neural information processing systems*, 32, 2019.
- Shivin Devgon, Jeffrey Ichnowski, Ashwin Balakrishna, Harry Zhang, and Ken Goldberg. Orienting novel 3d objects using self-supervised learning of rotation transforms. In *2020 IEEE 16th International Conference on Automation Science and Engineering (CASE)*, pp. 1453–1460. IEEE, 2020.

- Ben Eisner, Harry Zhang, and David Held. Flowbot3d: Learning 3d articulation flow to manipulate articulated objects. *arXiv preprint arXiv:2205.04382*, 2022.
- Asher Elmquist, Aaron Young, Thomas Hansen, Sriram Ashokkumar, Stefan Caldararu, Abhiraj Dashora, Ishaan Mahajan, Harry Zhang, Luning Fang, He Shen, et al. Art/atk: A research platform for assessing and mitigating the sim-to-real gap in robotics and autonomous vehicle engineering. *arXiv preprint arXiv:2211.04886*, 2022.
- Shai Feldman, Liran Ringel, Stephen Bates, and Yaniv Romano. Achieving risk control in online learning settings. *arXiv preprint arXiv:2205.09095*, 2022.
- Runyang Feng, Yixing Gao, Tze Ho Elden Tse, Xueqing Ma, and Hyung Jin Chang. Diffpose: Spatiotemporal diffusion model for video-based human pose estimation. In *Proceedings of the IEEE/CVF International Conference on Computer Vision*, pp. 14861–14872, 2023.
- Adam Fisch, Tal Schuster, Tommi Jaakkola, and Regina Barzilay. Few-shot conformal prediction with auxiliary tasks. In *International Conference on Machine Learning*, pp. 3329–3339. PMLR, 2021.
- Isaac Gibbs and Emmanuel Candès. Conformal inference for online prediction with arbitrary distribution shifts. *arXiv preprint arXiv:2208.08401*, 2022.
- Jia Gong, Lin Geng Foo, Zhipeng Fan, Qihong Ke, Hossein Rahmani, and Jun Liu. Diffpose: Toward more reliable 3d pose estimation. In *Proceedings of the IEEE/CVF Conference on Computer Vision and Pattern Recognition*, pp. 13041–13051, 2023.
- Albert Gu and Tri Dao. Mamba: Linear-time sequence modeling with selective state spaces. *arXiv preprint arXiv:2312.00752*, 2023.
- Jonathan Ho, Ajay Jain, and Pieter Abbeel. Denoising diffusion probabilistic models. *Advances in neural information processing systems*, 33:6840–6851, 2020.
- Jonathan Ho, Chitwan Saharia, William Chan, David J Fleet, Mohammad Norouzi, and Tim Salimans. Cascaded diffusion models for high fidelity image generation. *Journal of Machine Learning Research*, 23(47):1–33, 2022.
- Wenbo Hu, Changgong Zhang, Fangneng Zhan, Lei Zhang, and Tien-Tsin Wong. Conditional directed graph convolution for 3d human pose estimation. In *Proceedings of the 29th ACM International Conference on Multimedia*, pp. 602–611, 2021.
- Huang Huang, Satvik Sharma, Antonio Loquercio, Anastasios Angelopoulos, Ken Goldberg, and Jitendra Malik. Conformal policy learning for sensorimotor control under distribution shifts. *arXiv preprint arXiv:2311.01457*, 2023.
- Rongjie Huang, Zhou Zhao, Huadai Liu, Jinglin Liu, Chenye Cui, and Yi Ren. Prodiff: Progressive fast diffusion model for high-quality text-to-speech. In *Proceedings of the 30th ACM International Conference on Multimedia*, pp. 2595–2605, 2022.
- Catalin Ionescu, Dragos Papava, Vlad Olaru, and Cristian Sminchisescu. Human3. 6m: Large scale datasets and predictive methods for 3d human sensing in natural environments. *IEEE transactions on pattern analysis and machine intelligence*, 36(7):1325–1339, 2013.
- David Jin, Sushrut Karmalkar, Harry Zhang, and Luca Carlone. Multi-model 3d registration: Finding multiple moving objects in cluttered point clouds. *arXiv preprint arXiv:2402.10865*, 2024.
- Heeseung Kim, Sungwon Kim, and Sungroh Yoon. Guided-tts: A diffusion model for text-to-speech via classifier guidance. In *International Conference on Machine Learning*, pp. 11119–11133. PMLR, 2022.
- Alon Levkovitch, Eliya Nachmani, and Lior Wolf. Zero-shot voice conditioning for denoising diffusion tts models. *arXiv preprint arXiv:2206.02246*, 2022.
- Chen Li and Gim Hee Lee. Generating multiple hypotheses for 3d human pose estimation with mixture density network. In *Proceedings of the IEEE/CVF conference on computer vision and pattern recognition*, pp. 9887–9895, 2019.

- Chen Li and Gim Hee Lee. Weakly supervised generative network for multiple 3d human pose hypotheses. *arXiv preprint arXiv:2008.05770*, 2020.
- Wenhao Li, Hong Liu, Runwei Ding, Mengyuan Liu, Pichao Wang, and Wenming Yang. Exploiting temporal contexts with strided transformer for 3d human pose estimation. *IEEE Transactions on Multimedia*, 25:1282–1293, 2022a.
- Wenhao Li, Hong Liu, Hao Tang, Pichao Wang, and Luc Van Gool. Mhformer: Multi-hypothesis transformer for 3d human pose estimation. In *Proceedings of the IEEE/CVF Conference on Computer Vision and Pattern Recognition*, pp. 13147–13156, 2022b.
- Vincent Lim, Huang Huang, Lawrence Yunliang Chen, Jonathan Wang, Jeffrey Ichnowski, Daniel Seita, Michael Laskey, and Ken Goldberg. Planar robot casting with real2sim2real self-supervised learning. *arXiv preprint arXiv:2111.04814*, 2021.
- Vincent Lim, Huang Huang, Lawrence Yunliang Chen, Jonathan Wang, Jeffrey Ichnowski, Daniel Seita, Michael Laskey, and Ken Goldberg. Real2sim2real: Self-supervised learning of physical single-step dynamic actions for planar robot casting. In *2022 International Conference on Robotics and Automation (ICRA)*, pp. 8282–8289. IEEE, 2022.
- Tsung-Yi Lin, Michael Maire, Serge Belongie, James Hays, Pietro Perona, Deva Ramanan, Piotr Dollár, and C Lawrence Zitnick. Microsoft coco: Common objects in context. In *Computer Vision—ECCV 2014: 13th European Conference, Zurich, Switzerland, September 6–12, 2014, Proceedings, Part V 13*, pp. 740–755. Springer, 2014.
- Matthew Loper, Naureen Mahmood, Javier Romero, Gerard Pons-Moll, and Michael J Black. Smpl: A skinned multi-person linear model. In *Seminal Graphics Papers: Pushing the Boundaries, Volume 2*, pp. 851–866. 2023.
- Xianzheng Ma, Hossein Rahmani, Zhipeng Fan, Bin Yang, Jun Chen, and Jun Liu. Remote: Reinforced motion transformation network for semi-supervised 2d pose estimation in videos. In *Proceedings of the AAAI Conference on Artificial Intelligence*, volume 36, pp. 1944–1952, 2022.
- Julieta Martinez, Rayat Hossain, Javier Romero, and James J Little. A simple yet effective baseline for 3d human pose estimation. In *Proceedings of the IEEE international conference on computer vision*, pp. 2640–2649, 2017.
- Dushyant Mehta, Helge Rhodin, Dan Casas, Pascal Fua, Oleksandr Sotnychenko, Weipeng Xu, and Christian Theobalt. Monocular 3d human pose estimation in the wild using improved cnn supervision. In *2017 international conference on 3D vision (3DV)*, pp. 506–516. IEEE, 2017.
- Alex Nichol, Prafulla Dhariwal, Aditya Ramesh, Pranav Shyam, Pamela Mishkin, Bob McGrew, Ilya Sutskever, and Mark Chen. Glide: Towards photorealistic image generation and editing with text-guided diffusion models. *arXiv preprint arXiv:2112.10741*, 2021.
- Tuomas Oikarinen, Daniel Hannah, and Sohrab Kazerounian. Graphmdn: Leveraging graph structure and deep learning to solve inverse problems. In *2021 International Joint Conference on Neural Networks (IJCNN)*, pp. 1–9. IEEE, 2021.
- Chuer Pan, Brian Okorn, Harry Zhang, Ben Eisner, and David Held. Tax-pose: Task-specific cross-pose estimation for robot manipulation. *arXiv preprint arXiv:2211.09325*, 2022.
- Chuer Pan, Brian Okorn, Harry Zhang, Ben Eisner, and David Held. Tax-pose: Task-specific cross-pose estimation for robot manipulation. In *Conference on Robot Learning*, pp. 1783–1792. PMLR, 2023.
- Georgios Pavlakos, Xiaowei Zhou, Konstantinos G Derpanis, and Kostas Daniilidis. Coarse-to-fine volumetric prediction for single-image 3d human pose. In *Proceedings of the IEEE conference on computer vision and pattern recognition*, pp. 7025–7034, 2017.
- Dario Pavllo, Christoph Feichtenhofer, David Grangier, and Michael Auli. 3d human pose estimation in video with temporal convolutions and semi-supervised training. In *Proceedings of the IEEE/CVF conference on computer vision and pattern recognition*, pp. 7753–7762, 2019.

- Robin Rombach, Andreas Blattmann, Dominik Lorenz, Patrick Esser, and Björn Ommer. High-resolution image synthesis with latent diffusion models. In *Proceedings of the IEEE/CVF conference on computer vision and pattern recognition*, pp. 10684–10695, 2022.
- Cédric Rommel, Eduardo Valle, Mickaël Chen, Souhaïel Khalfaoui, Renaud Marlet, Matthieu Cord, and Patrick Pérez. Diffhpe: Robust, coherent 3d human pose lifting with diffusion. In *Proceedings of the IEEE/CVF International Conference on Computer Vision*, pp. 3220–3229, 2023.
- Chitwan Saharia, William Chan, Huiwen Chang, Chris Lee, Jonathan Ho, Tim Salimans, David Fleet, and Mohammad Norouzi. Palette: Image-to-image diffusion models. In *ACM SIGGRAPH 2022 conference proceedings*, pp. 1–10, 2022.
- Glenn Shafer and Vladimir Vovk. A tutorial on conformal prediction. *Journal of Machine Learning Research*, 9(3), 2008.
- Wenkang Shan, Haopeng Lu, Shanshe Wang, Xinfeng Zhang, and Wen Gao. Improving robustness and accuracy via relative information encoding in 3d human pose estimation. In *Proceedings of the 29th ACM International Conference on Multimedia*, pp. 3446–3454, 2021.
- Wenkang Shan, Zhenhua Liu, Xinfeng Zhang, Shanshe Wang, Siwei Ma, and Wen Gao. P-stmo: Pre-trained spatial temporal many-to-one model for 3d human pose estimation. In *European Conference on Computer Vision*, pp. 461–478. Springer, 2022.
- Wenkang Shan, Zhenhua Liu, Xinfeng Zhang, Zhao Wang, Kai Han, Shanshe Wang, Siwei Ma, and Wen Gao. Diffusion-based 3d human pose estimation with multi-hypothesis aggregation. In *Proceedings of the IEEE/CVF International Conference on Computer Vision*, pp. 14761–14771, 2023.
- Saurabh Sharma, Pavan Teja Varigonda, Prashast Bindal, Abhishek Sharma, and Arjun Jain. Monocular 3d human pose estimation by generation and ordinal ranking. In *Proceedings of the IEEE/CVF international conference on computer vision*, pp. 2325–2334, 2019.
- Sitian Shen, Zilin Zhu, Linqian Fan, Harry Zhang, and Xinxiao Wu. Diffclip: Leveraging stable diffusion for language grounded 3d classification. In *Proceedings of the IEEE/CVF Winter Conference on Applications of Computer Vision*, pp. 3596–3605, 2024.
- Khe Chai Sim, Françoise Beaufays, Arnaud Benard, Dhruv Guliani, Andreas Kabel, Nikhil Khare, Tamar Lucassen, Petr Zadrzil, Harry Zhang, Leif Johnson, et al. Personalization of end-to-end speech recognition on mobile devices for named entities. In *2019 IEEE Automatic Speech Recognition and Understanding Workshop (ASRU)*, pp. 23–30. IEEE, 2019.
- Jascha Sohl-Dickstein, Eric Weiss, Niru Maheswaranathan, and Surya Ganguli. Deep unsupervised learning using nonequilibrium thermodynamics. In *International conference on machine learning*, pp. 2256–2265. PMLR, 2015.
- Yang Song and Stefano Ermon. Improved techniques for training score-based generative models. *Advances in neural information processing systems*, 33:12438–12448, 2020.
- Yang Song, Jascha Sohl-Dickstein, Diederik P Kingma, Abhishek Kumar, Stefano Ermon, and Ben Poole. Score-based generative modeling through stochastic differential equations. *arXiv preprint arXiv:2011.13456*, 2020.
- David Stutz, Ali Taylan Cemgil, Arnaud Doucet, et al. Learning optimal conformal classifiers. *arXiv preprint arXiv:2110.09192*, 2021.
- Jiankai Sun, Yiqi Jiang, Jianing Qiu, Parth Nobel, Mykel J Kochenderfer, and Mac Schwager. Conformal prediction for uncertainty-aware planning with diffusion dynamics model. *Advances in Neural Information Processing Systems*, 36, 2024.
- Bugra Tekin, Artem Rozantsev, Vincent Lepetit, and Pascal Fua. Direct prediction of 3d body poses from motion compensated sequences. In *Proceedings of the IEEE Conference on Computer Vision and Pattern Recognition*, pp. 991–1000, 2016.

- Jacopo Teneggi, Matthew Tivnan, Web Stayman, and Jeremias Sulam. How to trust your diffusion model: A convex optimization approach to conformal risk control. In *International Conference on Machine Learning*, pp. 33940–33960. PMLR, 2023.
- Timo Von Marcard, Roberto Henschel, Michael J Black, Bodo Rosenhahn, and Gerard Pons-Moll. Recovering accurate 3d human pose in the wild using imus and a moving camera. In *Proceedings of the European conference on computer vision (ECCV)*, pp. 601–617, 2018.
- Tom Wehrbein, Marco Rudolph, Bodo Rosenhahn, and Bastian Wandt. Probabilistic monocular 3d human pose estimation with normalizing flows. In *Proceedings of the IEEE/CVF international conference on computer vision*, pp. 11199–11208, 2021.
- Yue Wu, Yongzhe Yuan, Xiaolong Fan, Xiaoshui Huang, Maoguo Gong, and Qiguang Miao. Pcrdiffusion: Diffusion probabilistic models for point cloud registration. *arXiv preprint arXiv:2312.06063*, 2023.
- Tianhan Xu and Wataru Takano. Graph stacked hourglass networks for 3d human pose estimation. In *Proceedings of the IEEE/CVF conference on computer vision and pattern recognition*, pp. 16105–16114, 2021.
- Heng Yang and Marco Pavone. Object pose estimation with statistical guarantees: Conformal key-point detection and geometric uncertainty propagation. In *Proceedings of the IEEE/CVF Conference on Computer Vision and Pattern Recognition*, pp. 8947–8958, 2023.
- Yupu Yao, Shangqi Deng, Zihan Cao, Harry Zhang, and Liang-Jian Deng. Apla: Additional perturbation for latent noise with adversarial training enables consistency. *arXiv preprint arXiv:2308.12605*, 2023.
- Ailing Zeng, Xiao Sun, Fuyang Huang, Minhao Liu, Qiang Xu, and Stephen Lin. Srnet: Improving generalization in 3d human pose estimation with a split-and-recombine approach. In *Computer Vision—ECCV 2020: 16th European Conference, Glasgow, UK, August 23–28, 2020, Proceedings, Part XIV 16*, pp. 507–523. Springer, 2020.
- Yu Zhan, Fenghai Li, Renliang Weng, and Wongun Choi. Ray3d: ray-based 3d human pose estimation for monocular absolute 3d localization. In *Proceedings of the IEEE/CVF Conference on Computer Vision and Pattern Recognition*, pp. 13116–13125, 2022.
- Haolun Zhang. Health diagnosis based on analysis of data captured by wearable technology devices. *International Journal of Advanced Science and Technology*, 95:89–96, 2016.
- Harry Zhang, Jeffrey Ichnowski, Yahav Avigal, Joseph Gonzales, Ion Stoica, and Ken Goldberg. Dex-net ar: Distributed deep grasp planning using a commodity cellphone and augmented reality app. In *2020 IEEE International Conference on Robotics and Automation (ICRA)*, pp. 552–558. IEEE, 2020.
- Harry Zhang, Jeffrey Ichnowski, Daniel Seita, Jonathan Wang, Huang Huang, and Ken Goldberg. Robots of the lost arc: Self-supervised learning to dynamically manipulate fixed-endpoint cables. In *2021 IEEE International Conference on Robotics and Automation (ICRA)*, pp. 4560–4567. IEEE, 2021.
- Harry Zhang, Ben Eisner, and David Held. Flowbot++: Learning generalized articulated objects manipulation via articulation projection. *arXiv preprint arXiv:2306.12893*, 2023.
- Jinlu Zhang, Yujin Chen, and Zhigang Tu. Uncertainty-aware 3d human pose estimation from monocular video. In *Proceedings of the 30th ACM International Conference on Multimedia*, pp. 5102–5113, 2022a.
- Jinlu Zhang, Zhigang Tu, Jianyu Yang, Yujin Chen, and Junsong Yuan. Mixste: Seq2seq mixed spatio-temporal encoder for 3d human pose estimation in video. In *Proceedings of the IEEE/CVF conference on computer vision and pattern recognition*, pp. 13232–13242, 2022b.
- Long Zhao, Xi Peng, Yu Tian, Mubbasir Kapadia, and Dimitris N Metaxas. Semantic graph convolutional networks for 3d human pose regression. In *Proceedings of the IEEE/CVF conference on computer vision and pattern recognition*, pp. 3425–3435, 2019.

Ce Zheng, Sijie Zhu, Matias Mendieta, Taojiannan Yang, Chen Chen, and Zhengming Ding. 3d human pose estimation with spatial and temporal transformers. In *Proceedings of the IEEE/CVF international conference on computer vision*, pp. 11656–11665, 2021.

Jieming Zhou, Tong Zhang, Zeeshan Hayder, Lars Petersson, and Mehrtash Harandi. Diff3dhpe: A diffusion model for 3d human pose estimation. In *Proceedings of the IEEE/CVF International Conference on Computer Vision*, pp. 2092–2102, 2023.

Xingyi Zhou, Qixing Huang, Xiao Sun, Xiangyang Xue, and Yichen Wei. Towards 3d human pose estimation in the wild: a weakly-supervised approach. In *Proceedings of the IEEE international conference on computer vision*, pp. 398–407, 2017.

A Coverage Guarantee and Empirical Coverage

Please refer to the standard proof shown in (Angelopoulos & Bates, 2021; Shafer & Vovk, 2008) for the coverage guarantees of conformal prediction.

To evaluate the empirical coverage of CHAMP, we calculate the mean coverage percentage across test data. Specifically, we use eq. (11) to check if the ground truth belongs in the confidence set formed by the conformity function on the test data:

$$\begin{aligned}\bar{c} &= \frac{1}{|I_{\text{test}}|} \sum_{\mathbf{y}_{\text{GT}} \sim I_{\text{test}}} \mathbb{1}(\mathbf{y}_{\text{GT}} \in C_{\theta}(\mathbf{y}, \tau)) \\ &= \frac{1}{|I_{\text{test}}|} \sum_{\mathbf{y}_{\text{GT}} \sim I_{\text{test}}} \mathbb{1}(\phi_{\theta}(\tilde{\mathbf{y}}, \mathbf{y}_{\text{GT}}) \geq \tau)\end{aligned}$$

We compare the three choices of conformity scores for the empirical coverage calculation. We use the test set from Human 3.6M and calculate the empirical coverage values across all activities. During training and testing, we keep $\alpha = 0.1$ for CP. From Fig. 7, we see the empirical coverage is

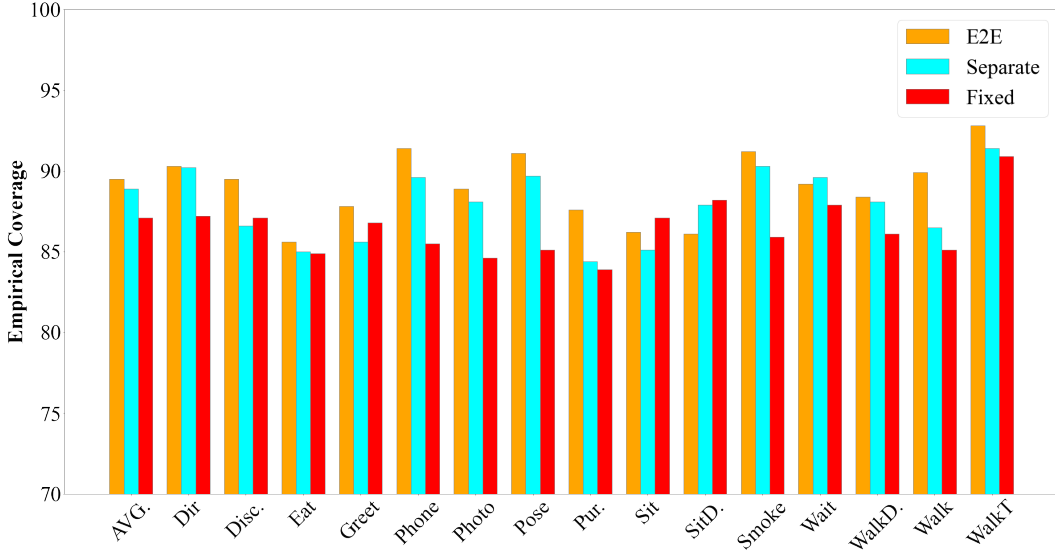


Figure 7: Empirical coverage comparison across three different conformity functions. We keep the best $\lambda = 0.05$ for comparison.

around $90\% \pm 5\%$ for all activities, which remains close to $1 - \alpha$, and in some cases, it exceeds this value. This is encouraging given the exchangeability assumption is not fully satisfied in our dataset.

B Denoiser in Training vs Inference

We first revisit DDIM (Song & Ermon, 2020). We start with the reverse process derivation and rewrite $q(\mathbf{y}_{t-1}|\mathbf{y}_t, \mathbf{y}_0)$ to be parameterized by a desired standard deviation σ_t :

$$\begin{aligned}\mathbf{y}_{t-1} &= \sqrt{\alpha_{t-1}}\mathbf{y}_0 + \sqrt{1 - \alpha_{t-1}}\boldsymbol{\epsilon}_{t-1} \\ &= \sqrt{\alpha_{t-1}}\mathbf{y}_0 + \sqrt{1 - \alpha_{t-1} - \sigma_t^2}\boldsymbol{\epsilon}_{t-1} + \sigma_t\boldsymbol{\epsilon} \\ &= \sqrt{\alpha_{t-1}}\left(\mathbf{y}_t - \sqrt{1 - \alpha_t}\boldsymbol{\epsilon}_{\theta}^{(t)}(\mathbf{y}_t)\right) + \sqrt{1 - \alpha_{t-1} - \sigma_t^2}\boldsymbol{\epsilon}_{\theta}^{(t)}(\mathbf{y}_t) + \sigma_t\boldsymbol{\epsilon} \\ &= \sqrt{\alpha_{t-1}}\left(\mathbf{y}_t - \sqrt{1 - \alpha_t}\boldsymbol{\epsilon}_{\theta}^{(t)}(\mathbf{y}_t)\right) + \sqrt{1 - \alpha_{t-1} - \sigma_t^2}\boldsymbol{\epsilon}_{\theta}^{(t)}(\mathbf{y}_t) + \sigma_t\boldsymbol{\epsilon}\end{aligned}$$

where the model $\epsilon_\theta^{(t)}(\cdot)$ predicts the ϵ_t from \mathbf{y}_t . Since $q(\mathbf{y}_{t-1}|\mathbf{y}_t, \mathbf{y}_0) = \mathcal{N}(\mathbf{y}_{t-1}; \mu(\mathbf{y}_t, \mathbf{y}_0), \beta_t \mathbf{I})$, therefore we have:

$$\tilde{\beta}_t = \sigma_t^2 = \frac{1 - \bar{\alpha}_{t-1}}{1 - \bar{\alpha}_t} \beta_t$$

Let $\sigma_t^2 = \eta \cdot \beta_t$ where η is a hyperparameter that controls the sampling stochasticity. During generation, we don't have to follow the whole chain $t = 1, \dots, T$, but only a subset of steps. Denote $t' < t$ as two steps in this accelerated trajectory. The DDIM update step is defined as follows:

$$q_{t', \theta}(\mathbf{y}_{t'}|\mathbf{y}_t, \mathbf{y}_0) = \mathcal{N}\left(\mathbf{x}_{t'}; \sqrt{\bar{\alpha}_{t'}}\left(\mathbf{y}_t - \sqrt{1 - \bar{\alpha}_t}\epsilon_\theta^{(t)}(\mathbf{y}_t)\right), \sigma_t^2 \mathbf{I}\right)$$

Following D3DP (Shan et al., 2023), the denoiser model D_θ uses DDIM to sample denoised poses from the corrupted ones. During training, we run DDIM for only 1 step for the sake of efficiency:

$$\bar{\mathbf{y}}^h = D_\theta(\mathbf{y}_T^h, \mathbf{x}, T), \mathbf{y}_T^h \sim \mathcal{N}(0, \mathbf{I}) \quad \forall h = \{1, \dots, H\}$$

During inference, we run DDIM for $K = 10$ times, and each step is defined as:

$$\begin{aligned} t &= T \cdot (1 - k/K), \quad t' = T \cdot (1 - (k+1)/K), \quad k = \{0, \dots, K-1\} \\ \bar{\mathbf{y}}^h &= D_\theta(\bar{\mathbf{y}}_t^h, \mathbf{x}, t), \quad \forall h = \{1, \dots, H\} \\ \bar{\mathbf{y}}_{t'}^h &= \sqrt{\bar{\alpha}_{t'}} \cdot \bar{\mathbf{y}}^h + \sqrt{1 - \bar{\alpha}_{t'} - \sigma_t^2} \cdot \epsilon_t + \sigma_t \epsilon \\ t &\leftarrow t' \end{aligned}$$

C Training-Calibration-Testing Data Split

We discuss the split of training, calibration, and testing data. We first split the testing data the same way as (Zhang et al., 2022b; Shan et al., 2023; Gong et al., 2023) to ensure the fairness of results. We then further split the training set into the actual training dataset and a calibration dataset before inference. Specifically, we split the training dataset by uniformly sampling a 2% subset as the calibration dataset, and CHAMP is only trained on the remaining 98%. Note here that this 2% calibration dataset is not seen during training by any means. During training, we split each mini-batch evenly into B_{pred} and B_{cal} .

D Architecture Details

We provide a more detailed version of Fig. 2. We illustrate the detailed architecture of the denoiser model D_θ as well as the conformity scoring model s_θ in Fig. 8. MixSTE (Zhang et al., 2022b) is used as the backbone of the denoiser. MixSTE combines 16 alternative spatial and temporal attention blocks. In the implementation, the channel size is set to 512. Similar to (Shan et al., 2023; Gong et al., 2023), we concatenate 2D keypoints and noisy 3D poses as inputs and add a diffusion timestep embedding after the input embedding using a sinusoidal function. For the conformity scoring model, we concatenate 2D keypoints and predicted hypotheses 3D poses as inputs, reuse the input embedding layer, and use an extra MLP layer to project the input embeddings into a lower dimension of 3. In training, CP is made differentiable by using soft ranking and soft assignment, resulting in a differentiable inefficiency loss $\mathcal{L}_{\text{ineff}}$. This loss is combined with the pose loss $\mathcal{L}_{\text{pose}}$ when back-propagating into the network. During inference (light cyan shaded area), we refine the hypotheses confidence set with regular CP on a held-out calibration set, resulting in $H' < H$ hypotheses. We then aggregate the refined set, resulting in a single final prediction.

E Procrustes-MPJPE Performance

The Procrustes MPJPE (P-MPJPE) metric, which is often referred to as Protocol #2, computes MPJPE after the estimated poses align to the ground truth using a rigid transformation. It is another standard metric for measuring a 3D pose estimator's performance (Pan et al., 2023). We report the

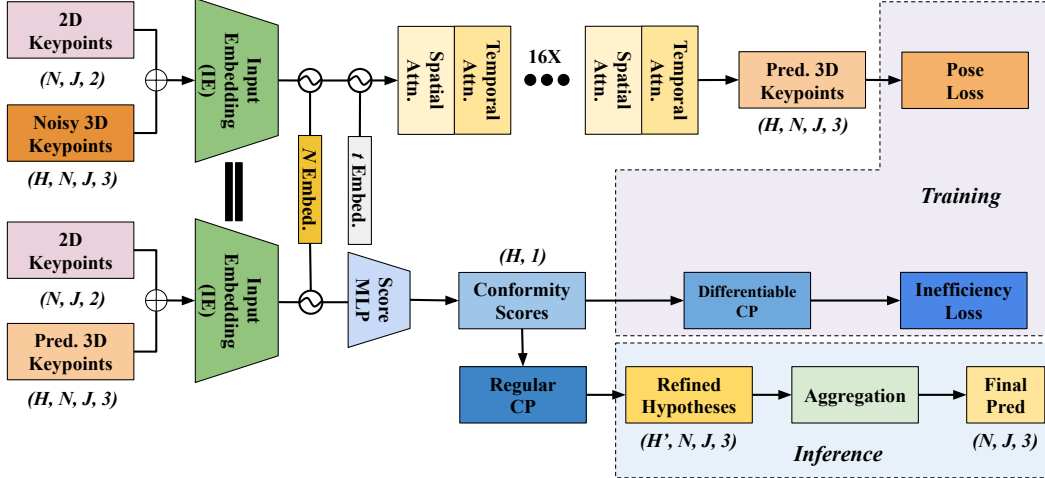


Figure 8: Detailed architecture of D_θ and s_θ , the denoiser and conformity score models during training and inference. During training, the construction of refined hypotheses set after differentiable CP is done via soft assignment. During inference, regular CP is used with the trained conformity score function.

performance of the four variants of CHAMP against other baselines on the Human3.6M dataset in Table 3. Quantitative results suggest our method achieves SOTA performance on this metric as well.

Procrustes Per-Joint Position Error (Protocol # 2) - mm																
	AVG.	Dir	Disc.	Eat	Greet	Phone	Photo	Pose	Pur.	Sit	SitD.	Smoke	Wait	WalkD.	Walk	WalkT.
Single Hypothesis																
STE Li et al. (2022a)	35.2	32.7	35.5	32.5	35.4	35.9	41.6	33.0	31.9	45.1	50.1	36.4	33.5	35.1	23.9	25.0
P-STMO Shan et al. (2022)	34.4	31.3	35.2	32.9	33.9	35.4	39.3	32.5	31.5	44.6	48.2	36.3	32.9	34.4	23.8	23.9
MixSTE Zhang et al. (2022b)	32.6	30.8	33.1	30.3	31.8	33.1	39.1	31.1	30.5	42.5	44.5	34.0	30.8	32.7	22.1	22.9
DUE Zhang et al. (2022a)	32.5	30.3	34.6	29.6	31.7	31.6	38.9	31.8	31.9	39.2	42.8	32.1	32.6	31.4	25.1	23.8
D3DP Shan et al. (2023)	31.7	30.6	32.5	29.1	31.0	31.9	37.6	30.3	29.4	40.6	43.6	33.3	30.5	31.4	21.5	22.4
CHAMP-Naive	31.2	30.9	32.1	29.4	30.9	31.2	35.9	29.4	28.9	40.1	41.9	33.1	30.0	30.8	20.9	22.4
Multiple Hypotheses																
MHFormer Li et al. (2022b)	34.4	34.9	32.8	33.6	35.3	39.6	32.0	32.2	43.5	48.7	36.4	32.6	34.3	23.9	25.1	34.4
GraphMDN Oikarinen et al. (2021)	46.9	39.7	43.4	44.0	46.2	48.8	54.5	39.4	41.1	55.0	69.0	49.0	43.7	49.6	38.4	42.4
DiffPose Choi et al. (2023)	39.9	35.9	40.3	36.7	41.4	39.8	43.4	37.1	35.5	46.2	59.7	39.9	38.0	41.9	32.9	34.2
DiffPose Gong et al. (2023)	28.7	26.3	29.0	26.1	27.8	28.4	34.6	26.9	26.5	36.8	39.2	29.4	26.8	28.4	18.6	19.2
DiffPose Feng et al. (2023)	32.0	28.1	31.5	28.0	30.8	33.6	35.3	28.5	27.6	40.8	44.6	31.8	32.1	32.6	28.1	26.8
D3DP-Agg Shan et al. (2023)	31.6	30.6	32.4	29.2	30.9	31.9	37.4	30.2	29.3	40.4	43.2	35.2	30.4	31.3	21.5	22.3
CHAMP-Naive	32.0	31.9	33.1	30.8	31.1	32.2	38.1	29.2	28.3	41.2	43.1	34.5	31.2	30.4	22.6	23.9
CHAMP	31.1	30.8	32.4	29.9	30.9	31.4	37.2	27.8	26.9	40.2	42.7	32.9	30.6	29.8	21.4	22.8
CHAMP-Agg	30.2	30.1	31.7	28.6	30.1	30.2	36.1	26.9	25.4	39.1	41.4	31.9	29.8	28.9	20.9	21.9
D3DP-Best* Shan et al. (2023)	28.7	27.5	29.4	26.6	27.7	29.2	34.3	27.5	26.2	37.3	39.0	30.3	27.7	28.2	19.6	20.3
CHAMP-Best*	28.5	28.9	30.1	27.2	27.3	28.2	34.4	24.7	24.1	37.2	38.9	29.9	28.1	27.1	20.1	19.9

Table 3: P-MPJPE (\downarrow) results on Human-3.6M dataset. *Upper-bound performance, needs ground truth.

F More Qualitative Results on In-the-Wild Videos

We showcase the performance of CHAMP on more in-the-wild videos in this section. We collect various YouTube and TikTok videos and detect 2D keypoints with Cascaded Pyramid Network. Note that the official weights provided by CPN are trained in COCO format, so we used a fine-tuned version of the weights for Human3.6M universal skeleton format. With such 2D keypoints, we are able to directly use the model trained on Human3.6M dataset and apply it to real-world videos without any fine-tuning. In Fig. 9, for each row, we show two examples. For every three images, the leftmost image is the RGB observation, and the middle image is all the hypotheses proposed by CHAMP’s pose estimation backbone, and the rightmost image is the hypotheses set refined by the learned conformal predictor.

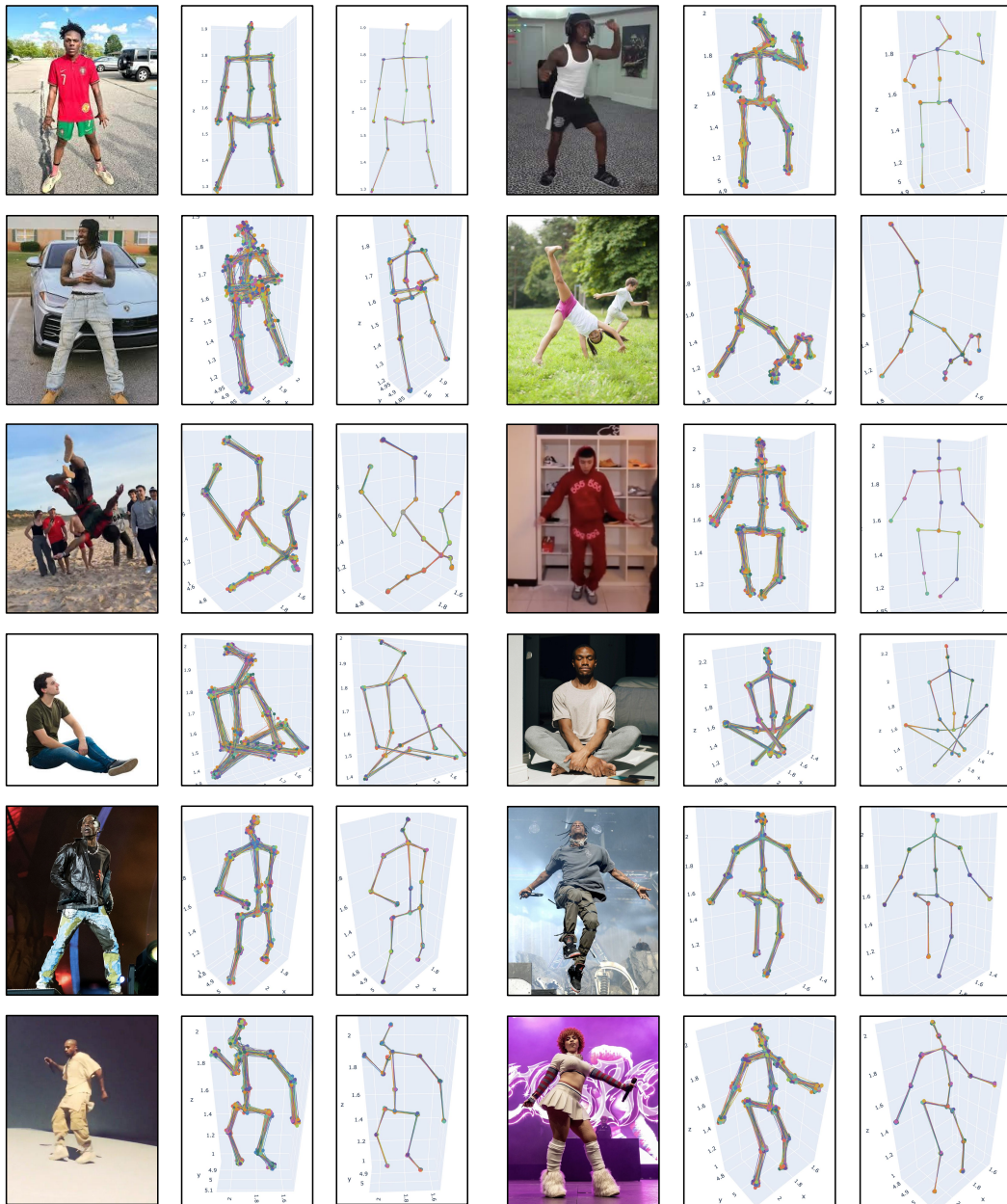


Figure 9: Results of running CHAMP on in-the-wild videos collected from TikTok and YouTube.

G Learned CP in CHAMP

We provide more demonstrations on the learned conformal predictor in CHAMP. Specifically, in Fig. 10, we provide more examples of predicted hypotheses before and after the conformal predictor powered by the learned score function.

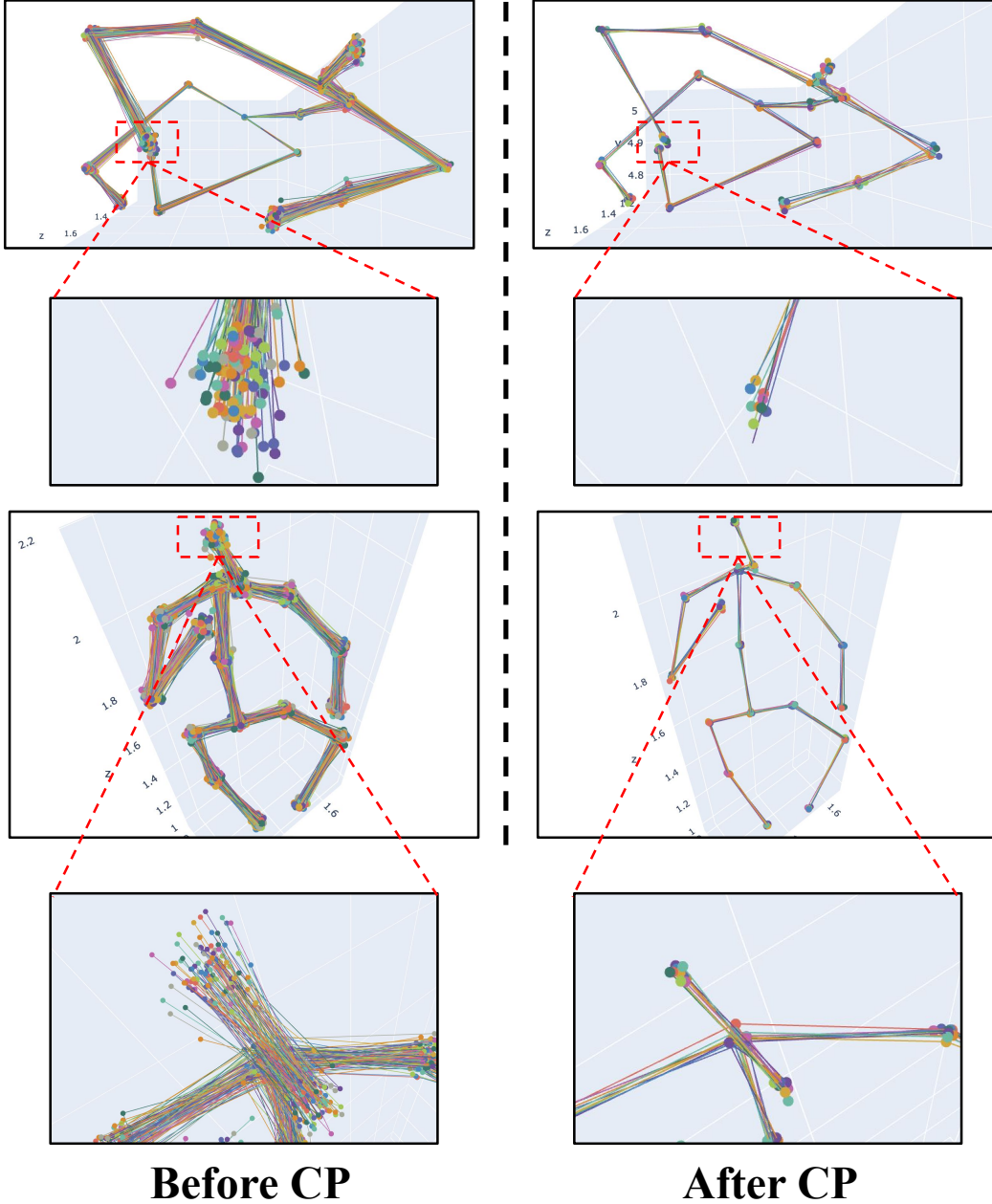


Figure 10: Examples of CP in CHAMP filtering out bad hypotheses during inference. Qualitatively, the learned score function filters out outlier predictions.